Research Article

Yali Zhang, Xiaosong Jiang*, Hongliang Sun, and Zhenyi Shao

Effect of annealing heat treatment on microstructure and mechanical properties of nonequiatomic CoCrFeNiMo medium-entropy alloys prepared by hot isostatic pressing

https://doi.org/10.1515/ntrev-2020-0047
received April 26, 2020; accepted May 17, 2020

Abstract: In this study, nonequiatomic $Co_{28.5}Cr_{21.5}Fe_{20}Ni_{26}Mo_4$ medium-entropy alloys (MEAs) were prepared using hot isostatic pressing. The effect of annealing heat treatment on microstructure and mechanical properties of MEAs was investigated. The results showed that the microstructure of as-sintered alloys was mainly composed of the face-centered cubic (FCC) phase and μ phase. The presence of the μ phase could improve the compressive strength of $Co_{28.5}Cr_{21.5}Fe_{20}Ni_{26}Mo_4$ MEAs. Meanwhile, the ductile FCC phase matrix could effectively suppress the propagation of cracks to improve its ductility. Hence, as-sintered MEAs possessed excellent compression properties, and the average compressive strength value was 2,606 MPa when the strain was 50%. Compared with as-sintered MEAs, the phase composition of as-annealed MEAs did not change. The micro-hardness of annealed MEAs was stable compared to as-sintered MEAs (342 HV), and its fluctuation was about ±30 HV. The compressive strength of the annealed MEAs did not alter greatly, and the maximum fluctuation value was only about 6.5%. Hence, $Co_{28.5}Cr_{21.5}Fe_{20}Ni_{26}Mo_4$ MEAs had excellent thermal stability.

Keywords: CoCrFeNiMo MEAs, annealing heat treatment, thermal stability

1 Introduction

Compared with traditional alloys [1,2], high entropy alloys (HEAs), which is a new alloy system, are easier to form simple solid solution such as FCC and body-centered cubic (BCC) rather than intermetallic compound phases [3,4]. They possessed strong structural stability, good corrosion resistance, excellent wear resistance, and high strength [5,6]. Among HEAs, CoCrFeNi-based alloys with the FCC structure possessed excellent tensile ductility and fracture toughness at ambient temperature and low temperature, while their strength was poor. However, the optimization of their performance could be achieved by adding other metal elements [7]. For instance, for CoCrFeMnNi HEAs, the addition of the Mn element resulted in that their microstructure consisted of a single phase of the FCC structure. Hence, the HEAs had excellent tensile strength, fracture toughness, as well as good toughness at low temperatures [8,9]. The $CoCrFeNiTa_x$ HEAs composed of the γ phase of the FCC structure and C14 type Laves phase of the HCP structure exhibited relatively high strength and high plasticity [10]. The yield strength of $CoCrFeNiNb_{0.25}$ HEAs increased sharply because of the addition of the Nb element, which was caused by the precipitation strengthening of ductile FCC precipitate with nano basket-weave microstructure, while the ductility of the HEAs slightly decreased [11]. Owing to the addition of the Al element, $Al_{0.3}CoCrFeNi$ HEAs produced nanocrystalline reaction with reduced contamination levels during mechanically activated annealing [12]. Experimental results about NiCoFeCrGa showed that the cooling rate could lead to a self-similarity of the solidified structure formed in the specimen and confirmed the grouping of Co, Fe, and Cr in the FCC phase [13]. Moreover, two elements were added to the CoCrFeNi-based alloys to form some novel HEAs [7], such as AlCoCrFeNbNi [14], $Al_{0.6}CrFeCoNiSi_{0.3}$ [15], and $Al_{0.5}CoCrFexNiTi_{0.5}$ [16], whose microstructure and mechanical properties had been extensively studied.

Among CoCrFeNi-based HEAs, the study of equiatomic CoCrFeNiMo HEAs is extremely attractive. The

* **Corresponding author: Xiaosong Jiang,** Key Laboratory of Advanced Technologies of Materials, Ministry of Education, Chengdu 610031, China; School of Materials Science and Engineering, Southwest Jiaotong University, Chengdu, Sichuan 610031, China, e-mail: xsjiang@swjtu.edu.cn, tel: +86-28-87600779, fax: +86-28-87600779
Yali Zhang, Hongliang Sun, Zhenyi Shao: Key Laboratory of Advanced Technologies of Materials, Ministry of Education, Chengdu 610031, China; School of Materials Science and Engineering, Southwest Jiaotong University, Chengdu, Sichuan 610031, China

properties of CoCrFeNi alloy could be effectively improved by precipitation strengthening caused by the addition of Mo element with a medium atomic size [17]. In terms of CoCrFeNiMo HEAs, their microstructure is mainly composed of solid solution phases of the FCC structure, σ phase and μ phase, and the regulation of these phases is the key to alter their properties. Wu et al. [18] added Mo element to CoCrFeNi alloy and found that the content of Mo element in $CoCrFeNiMo_x$ HEAs could affect the formation of the σ phase and μ phase, which could change the microstructure and properties of HEAs. Due to the addition of the Mo element, $CrFeCoNiMo_{0.2}$ HEAs got high activation energy (463 kJ mol^{-1}), and their phases could be separated during thermal deformation [19]. In addition, during the process of dynamic recrystallization, Mo-rich phase particles formed in HEAs could restrict the migration on grain boundary by the pinning effect to improve the size of the recrystallized grains. Cai et al. [20] found that the annealed $FeCoCrNiMo_{0.23}$ HEAs could produce Mo-rich intermetallic particles and reduced the stacking fault probability, resulting in the enhancement of their strength and the decrease of their ductility. It was indicated that the microalloying of Mo element could increase the strength of the alloys. The low ductility of $FeCoCrNiMo_{0.23}$ HEAs was mainly attributed to the weak bond between the particles and the matrix interface as well as the reduction of the stacking fault probability, which could inhibit the formation of deformed twins. The microstructure of as-cast $CoCrFeNiMo_{0.85}$ HEAs was studied by Shun et al. [21], and their microstructure consisted of the FCC phase, a (Mo, Cr)-rich σ phase, and a minor (Mo, Cr)-rich μ phase. After $CoCrFeNiMo_{0.85}$ HEAs were processed by the aging treatment at 700°C, their hardness was optimal, which was caused by the precipitation of acicular σ phase in the FCC phase matrix. Similarly, in the study on $CoCrFeNiMo_x$ HEAs [22], it was found that the hardness of the FCC phase and σ phase was enhanced with the increment of Mo element in the alloys, which increased the hardness of HEAs. Meanwhile, with the increasing of Mo element, the compression resistance of HEAs was improved, while their ductility was reduced. Hence, it can be found that the equiatomic CoCrFeNiMo HEAs have high hardness and strength, but their ductility still needs to be further improved.

Recently, the novel nonequiatomic CoCrFeNiMo MEAs, whose microstructures were mainly composed of the FCC phase and μ phase, had been proposed, and they exhibited excellent tensile strength and ductility [23]. The properties of the $Co_{18}Cr_{12.5}Fe_{55}Ni_7Mo_{7.5}$ MEAs could be enhanced by the formation of the μ phase, which could result in the precipitation strengthening, the inhibition of grain growth, as well as recrystallization by the Zener pinning effect. Compared with other preparation techniques [24–26], hot isostatic pressing technology possesses the advantages of low forming temperature, compact product, excellent performance, etc. [27], and so it is applied to fabricate the $Co_{28.5}Cr_{21.5}Fe_{20}Ni_{26}Mo_4$ MEAs in this experiment. At the same time, to explore the thermal stability of MEAs, the effect of the annealing heat treatment with diverse annealing temperatures (500, 550, 600, 800, 850, 900, 1,100, 1,150, and 1,200°C) on the microstructure and properties of the MEAs was investigated [28]. Subsequently, the microstructure and the mechanical properties of $Co_{28.5}Cr_{21.5}Fe_{20}Ni_{26}Mo_4$ MEAs (as-sintered and as-annealed) were analyzed in detail. Furthermore, the formation mechanism of nonequiatomic $Co_{28.5}Cr_{21.5}Fe_{20}Ni_{26}Mo_4$ MEAs prepared by hot isostatic pressing and their thermal stability were discussed.

2 Experimental procedure

2.1 Materials preparation

In this study, the alloy ingot with the nominal composition of $Co_{28.5}Cr_{21.5}Fe_{20}Ni_{26}Mo_4$ was fabricated by the hot isostatic pressing technology (HIP) under an Ar atmosphere using the pre-alloying powder that was prepared by atomization. The original powder was supplied by SANDVIK Coromant. High-purity Fe, Co, Cr, Ni, and Mo (20:28.5:21.5:26:4) powders were melted in an induction-heated vacuum furnace to ensure the uniformity of powders, and the melt was dropped using a ceramic tube. The liquid droplets flew in the atomization chamber under high purity Ar (4 MPa), and then solidified to powders with the decrease of temperature. The $Co_{28.5}Cr_{21.5}Fe_{20}Ni_{26}Mo_4$ MEAs with high density and low porosity were successfully fabricated. First, the temperature was increased from 20 to 650°C at a rate of 15°C min^{-1}, and the pressure was increased to 20 MPa. Second, the temperature was increased to 11,90°C at a rate of 5°C min^{-1}, and the pressure was increased to 150 MPa. Third, the pressure was maintained at 150 MPa, and the temperature was maintained at 1,190°C with 2.5 h. Finally, the temperature was decreased to ambient temperature at a rate of 10°C min^{-1}, and the pressure was decreased to 40 MPa. After the pressure was released, the specimens were taken out of the chamber. The process curve is shown in Figure 1.

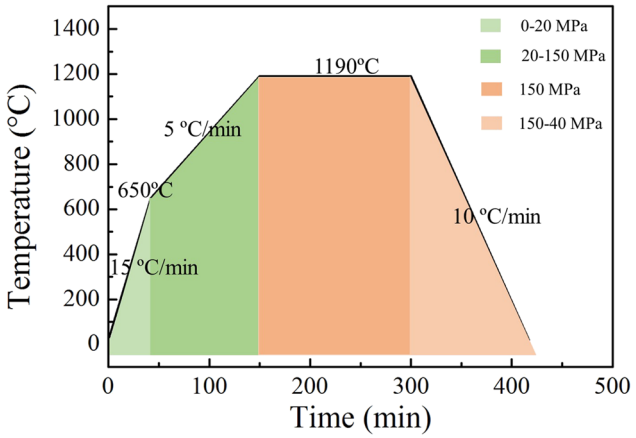

Figure 1: The sintered process curve.

Table 1: The parameters of the annealing process

Specimens	Temperature/°C	Holding time/h
N-HT	As-sintered	—
H-120	1,200	4
H-115	1,150	4
H-110	1,100	4
M-90	900	4
M-85	850	4
M-80	800	4
L-60	600	4
L-55	550	4
L-50	500	4

2.2 Heat treatment

The $Co_{28.5}Cr_{21.5}Fe_{20}Ni_{26}Mo_4$ MEAs prepared by hot isostatic pressing sintering were cut using the DK7740 CNC wire-cut electrical discharge machining (EDM) machine, and the dimension of the specimens was 15 mm × 15 mm × 5 mm. The surface of specimens was cleaned with acetone as well as alcohol and dried in air. Subsequently, the specimens were placed in an HVS-25 type vacuum sintering furnace that possesses the degree of vacuum of 6.6×10^{-3} Pa to conduct the annealing heat treatment and prevent oxidation of the specimens. In this experiment, to study the influence of annealing temperature on the microstructure of the MEAs, the specimens were treated with different annealing temperatures under the identical holding time of 4 h. The annealing parameters are summarized in Table 1. First, the temperature was increased to 100°C at a heating rate of 5°C min^{-1}. Second, the temperature was increased to the required holding temperature at a heating rate of 10°C min^{-1}. Then, a holding time of 240 min was applied. Finally, the temperature was decreased to 800°C at a cooling rate of 10°C min^{-1}, and then, the specimens were taken out after the temperature naturally decreased to room temperature.

2.3 Materials characterization

Scanning electron microscopy (SEM; 10 kV, JEOL, JSM7800f) was used to observe and analyze the microstructure of the raw powder and $Co_{28.5}Cr_{21.5}Fe_{20}Ni_{26}Mo_4$ MEAs. At the same time, the phase composition of the raw powder and $Co_{28.5}Cr_{21.5}Fe_{20}Ni_{26}Mo_4$ MEAs was confirmed by X-ray diffraction (XRD; X. Pert Pro-MPD). The variation of chemical composition in the $Co_{28.5}Cr_{21.5}Fe_{20}Ni_{26}Mo_4$ MEAs was analyzed using energy dispersion spectroscopy (EDS, 20 kV). The Vickers micro-hardness tester (HVS-30) was used to perform the micro Vickers hardness test with a testing load of 200 g and a dwell time of 15 s. Meanwhile, the compression strength of MEAs was evaluated using the electronic universal testing machine, and a loading rate of 0.5 mm min^{-1} at ambient temperature was applied. The dimension of specimens was 7 × 5 × 5 mm^3, and three specimens were tested under each condition.

3 Results and discussions

3.1 Microstructure of $Co_{28.5}Cr_{21.5}Fe_{20}Ni_{26}Mo_4$ MEA powder

Figure 2a shows that most of the powders are spherical, and the shapes of some powder are short rod shape and ellipsoid shape. The diameter of the spherical powder is about 20–40 μm. One of the spherical powders is analyzed by SEM and EDS, and the results are shown in Figure 2b–f. The Fe, Co, Ni, Cr, and Mo elements are uniformly distributed in the powder, indicating that the quality of the pre-alloyed powder is ideal. In addition, spot scanning tests of EDS are conducted on the powder, and the results show that the powder is mainly composed of Co (29.1 ± 0.5 at%), Cr (20.7 ± 0.4 at%), Fe (20.4 ± 0.7 at%), Ni (25.4 ± 0.5 at%), and Mo (4.4 ± 0.6 at%) elements. There is a slight difference between the practical proportion of elements in the powder and the nominal proportion of the powder, indicating that the elemental ratio of the pre-alloyed powder is ideal. The original powder is analyzed by the XRD test, and the results are shown in Figure 3. The microstructure of the powder is composed of the FCC phase and FeO.

Similarly, Mu et al. [29] also found that the FCC phase existed in the CoCrFeNiMo alloy powder. During the preparation of the pre-alloy powder, a small amount of Fe element is susceptible to react with oxygen to generate some FeO at high temperature. In addition, the FCC phase exhibits low strength and good plasticity, while the BCC phase exhibits high strength and high brittleness. Hence, FCC and/or BCC formed in HEAs has an important role in the performance of the alloys [30].

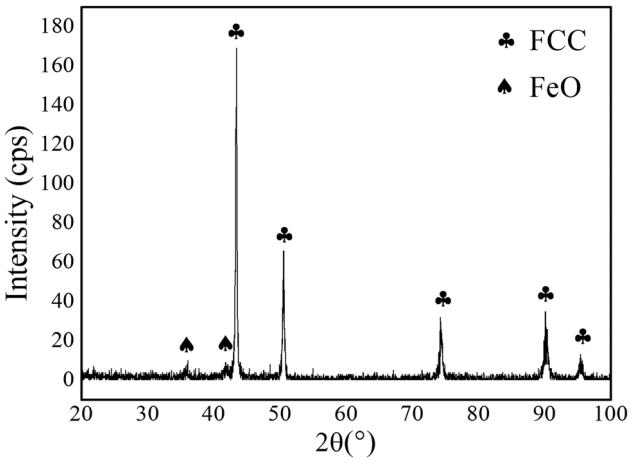

Figure 3: The XRD pattern of $Co_{28.5}Cr_{21.5}Fe_{20}Ni_{26}Mo_4$ MEAs powder.

3.2 XRD analysis of $Co_{28.5}Cr_{21.5}Fe_{20}Ni_{26}Mo_4$ MEAs

The XRD patterns of as-sintered and as-annealed $Co_{28.5}Cr_{21.5}Fe_{20}Ni_{26}Mo_4$ MEAs are shown in Figure 4. The phase composition of alloys mainly comprised the FCC phase and topologically close-packed μ phase ($R3m$). According to the JCPDS card number 29-0489, the structure of the μ phase is similar to rhombohedral Co_7Mo_6 phase (a = 4.762 Å, b = 4.762 Å, c = 25.617 Å) [22]. Among as-sintered and as-annealed alloys, the dominant phase is the FCC phase. Due to the existence of the high entropy effect, the Gibbs free energy in the alloys can be reduced to promote the formation of FCC solid solution during solidification. The mixing entropy plays an important role in the process of preparing multi-component alloys under high-temperature conditions. When the mixing entropy increases, the formation of solid solution phase can be promoted and the formation of intermetallic phases can be inhibited [5]. The calculation of the mixing entropy will be carried out in Section 4.

In the past studies, most of the binary components crystallize in the alloys with the FCC structure to form the FCC phase, such as CoNi, CoFe, and FeNi. Moreover, the stability of the FCC phase in the alloys can be enhanced by the complete dissolution of CoNi and FeNi [8,31–33]. The phase transition of HEAs is not primarily influenced by individual elements, while it is largely controlled by the previous evolutionary binary components. It was found that CoCrFeNiMo HEAs contained binary components with the FCC structure, such as CoNi, NiCr, NiFe, and NiMo [34]. Therefore, the formation of the FCC phase in $Co_{28.5}Cr_{21.5}Fe_{20}Ni_{26}Mo_4$ MEAs can be stabilized by the mutual dissolution of similar binary

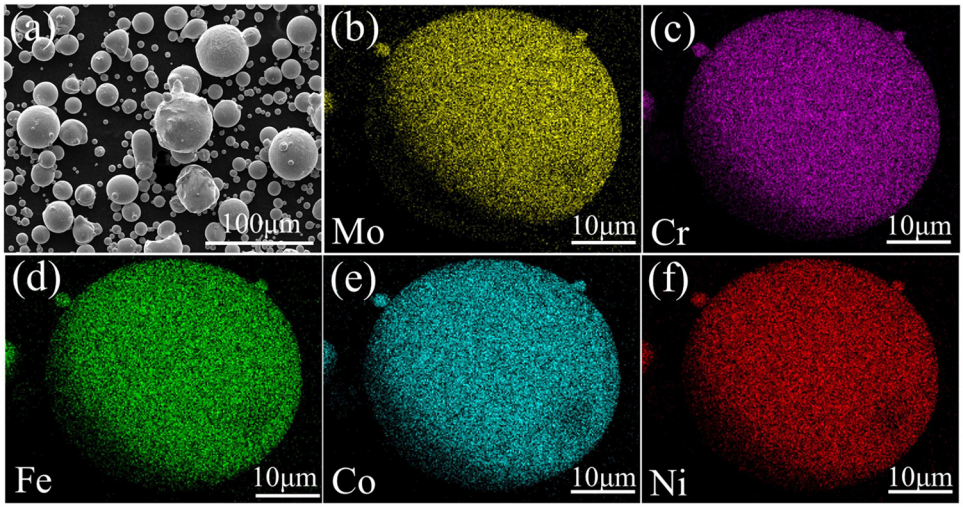

Figure 2: (a) SEM image of $Co_{28.5}Cr_{21.5}Fe_{20}Ni_{26}Mo_4$ MEAs powders, (b) distribution of Mo element, (c) distribution of Cr element, (d) distribution of Fe element, (e) distribution of Co element, and (f) distribution of Ni element.

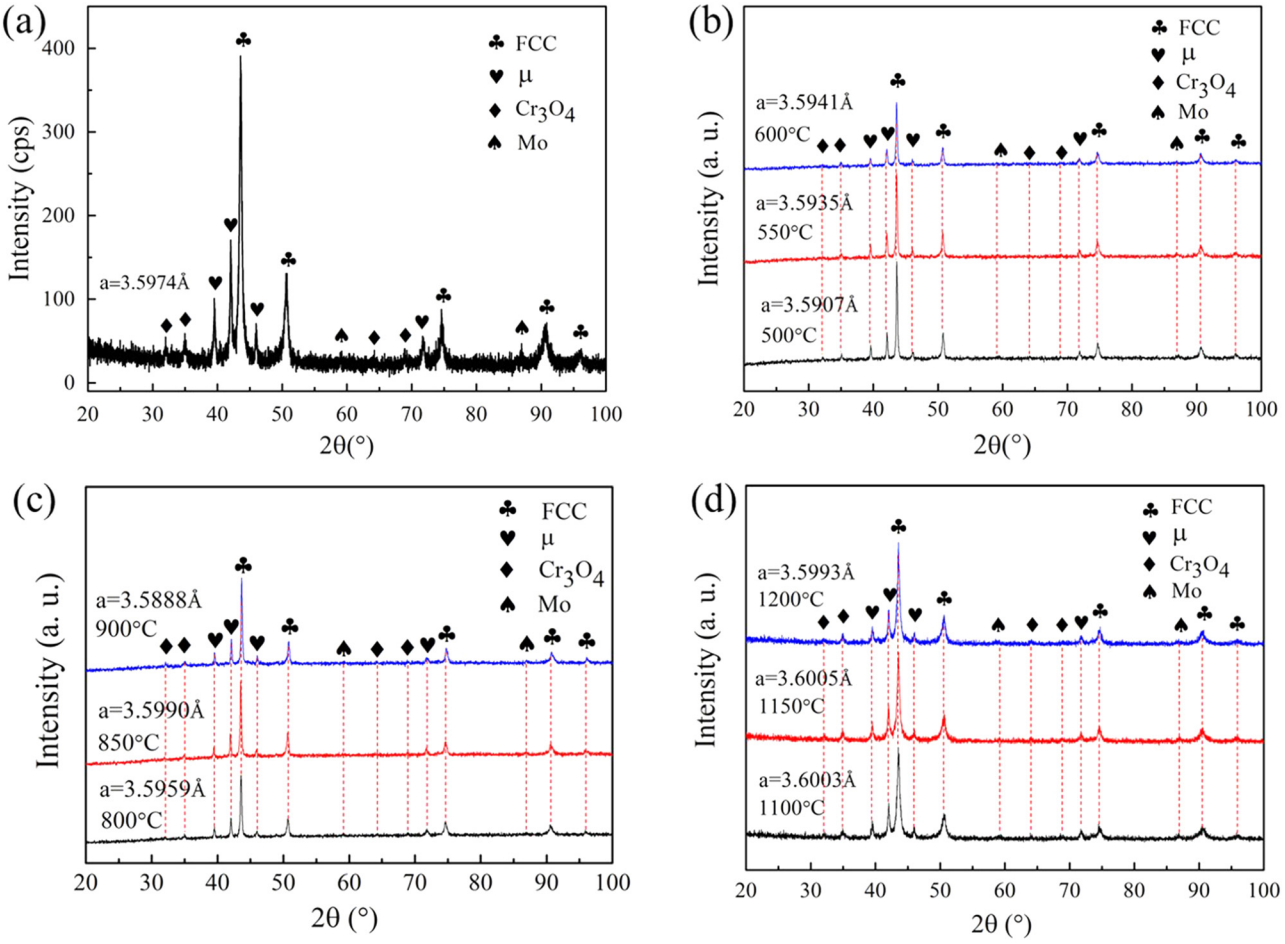

Figure 4: The XRD patterns of as-sintered and as-annealed alloys: (a) N-HT alloy, (b) L-50 alloy; L-55 alloy; L-60 alloy, (c) M-80 alloy; M-85 alloy; M-90 alloy, and (d) H-110 alloy; H-115 alloy; H-120 alloy.

components. Liu et al. [17] found that the strength of CoCrFeNiMo HEAs could be significantly enhanced by the incoherent intermetallic phase (μ phase), and severe embrittlement of alloys did not occur. According to the previous studies, it was found that the μ phase was a (Mo, Cr)-rich phase in which the Mo content was greater than the Cr content [18]. Similarly, both Wang et al. [19] and Cai et al. [20] also found a Mo-rich phase in the Fe–Co–Ni–Cr–Mo alloys. According to the XRD patterns, compared with the as-sintered alloys, the position of the diffraction peak of each phase almost does not alter with the increase of the annealing temperature, indicating that the phase composition of the alloys does not change. Hence, the transition of the FCC phase to the BCC phase does not occur during quasi-equilibrium solidification. In addition, the FCC phase can be detected in the alloys annealed at high temperatures, indicating that the FCC phase can stably exist in the alloys over the range of high temperature [35]. Therefore, the annealing heat treatment does not promote the occurrence of phase transition in $Co_{28.5}Cr_{21.5}Fe_{20}Ni_{26}Mo_4$ MEAs, and similar phenomena had been found in other results [23,36]. In addition, a small amount of Cr oxides (Cr_3O_4) are discovered, which may be produced during high-temperature sintering. A small amount of Mo solid solution is found, which is mainly attributed to the low diffusivity of Mo.

The lattice parameters of the FCC matrix for as-sintered and as-annealed $Co_{28.5}Cr_{21.5}Fe_{20}Ni_{26}Mo_4$ MEAs are calculated by using Maud software, and the results are shown in Figure 5. The lattice parameter for as-sintered MEAs is 3.5974 Å, and the lattice parameter for L-50 to M-85 alloy is found to increase gradually from 3.5907 to 3.599 Å. However, the lattice parameter for M-90 alloy significantly decreases to 3.5888 Å, and then, the lattice parameter for H-110 alloy increases to 3.6003 Å. In terms of H-115 alloy and H-120 alloy, the lattice parameter is similar to H-110 alloy. To further

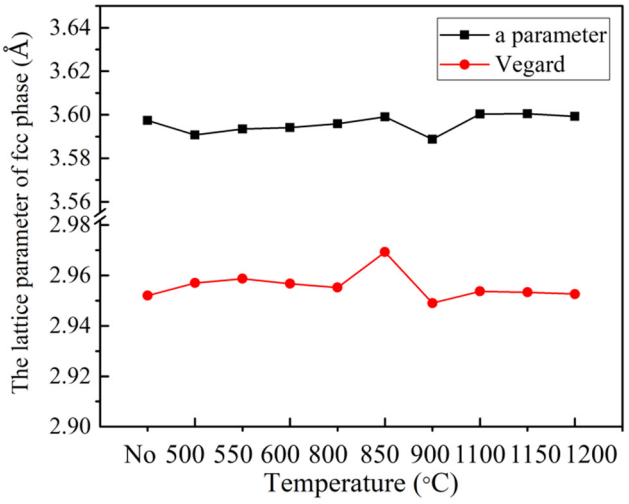

Figure 5: The lattice parameters of the FCC matrix for as-sintered and as-annealed $Co_{28.5}Cr_{21.5}Fe_{20}Ni_{26}Mo_4$ MEAs.

study the change of the lattice parameter, the rule of mixtures (Equation (1)) is used to calculate the theoretical lattice parameter of the FCC matrix for MEAs, and the results are also shown in Figure 5 [37]. Compared with the lattice parameter calculated by applying Maud software, the theoretical lattice parameter of the FCC matrix for all MEAs is relatively low. Because Equation (1) is just used to obtain a rough theoretical lattice parameter, the calculation of the theoretical lattice parameter of the FCC phase can be better finished by the usage of first principle [38]. Similarly, the theoretical lattice parameter of the FCC matrix for M-85 alloy is the highest (2.9693 Å), and the theoretical lattice parameter for M-90 alloy also significantly decreases to 2.9490 Å.

$$a_{\text{mix}} = \sum c_i a_i \tag{1}$$

where c_i is the atomic fraction of the ith element and a_i is the lattice parameter of the ith element.

The change of the lattice parameter is caused by the change of the ratio among the solid solution atoms in the FCC phase during the heat treatment. Since the atomic radius of the Mo element is larger than the atomic radius of the other elements, the movement of Mo atoms is more likely to cause lattice expansion during heat treatment [22]. Furthermore, the diminishing of the lattice parameter for as-annealed alloys is caused by desolution and renovation in the solid solution phase during the sintering. The precipitation of the metal component is too violent, so that the deformation energy is released, resulting in a decrease in lattice parameters [39].

3.3 Microstructure of $Co_{28.5}Cr_{21.5}Fe_{20}Ni_{26}Mo_4$ MEAs

The microstructure of as-sintered $Co_{28.5}Cr_{21.5}Fe_{20}Ni_{26}Mo_4$ MEAs is observed by the SEM-BSE analysis, and the results are shown in Figure 6. It is found that the distribution of the μ phase grains is uneven, and the grain size of the μ phase is greatly different from each other. Certain regions are composed of small and dense grains (red dotted circle), and most areas mainly consist of large and sparse grains. The chemical composition of the FCC phase and μ phase is analyzed by the SEM-EDS. The results show that the FCC phase (region II) is mainly composed of Fe (21.3 ± 0.6 at%), Co (28.2 ± 0.7 at%), Ni (25.6 ± 0.9 at%), Cr (21.7 ± 0.4 at%), and Mo (3.2 ± 0.3 at%) elements, while the μ phase (region I) mainly consists of Fe (11.0 ± 0.5 at%), Co (20.6 ± 0.6 at%), Ni (15.6 ± 0.8 at%), Cr (20.6 ± 0.5 at%), and Mo (32.2 ± 0.4 at%) elements. At high temperature, an element possessing high melting point has high diffusion activation energy and low diffusion rate. Hence, the diffusion ability of the Mo element with a high melting point is poor, which results in the occurrence of a serious segregation phenomenon of Mo element as well as the generation of a large number of small μ phase grains [40]. Similarly, the aggregated nanoparticle phase was found in the AlCrFeNiTi$_{0.5}$ HEAs, and the nanoparticle phase disappeared with the increase in the annealing temperature [41]. As shown in Figures 8 and 9, this aggregation phenomenon is not found in the alloys at diverse annealing temperatures. Therefore, the aggregated μ phase grains appearing in the as-sintered alloy can be eliminated by the annealing heat treatment.

The irregular black-gray region is found in $Co_{28.5}Cr_{21.5}Fe_{20}Ni_{26}Mo_4$ MEAs, as shown in Figure 6c. This region mainly consists of dark-gray phase and light-gray phase. The SEM-EDS tests are performed on these phases, and the results are shown in Figure 7. It is found that the irregular black-gray region is composed of O, Cr, and Mo elements. O and Cr elements mainly concentrate in the dark-gray phase, and the Mo element is mainly distributed in the light-gray phase. Combined with the previous XRD analysis, the black-gray phase is Cr oxide (Cr_3O_4). Karlsdottir et al. [34] also found Cr oxides in CoCrFeNiMo HEAs. Hence, the irregular region is mainly composed of Cr oxides and a small amount of Mo solid solution. The Cr_3O_4 may be generated by the existence of a little oxygen during sintering. The existence of Cr_3O_4 can effectively prevent the occurrence of serious wear when the alloy is applied in industry and can lubricate the friction process between the alloy surface and the friction material [42].

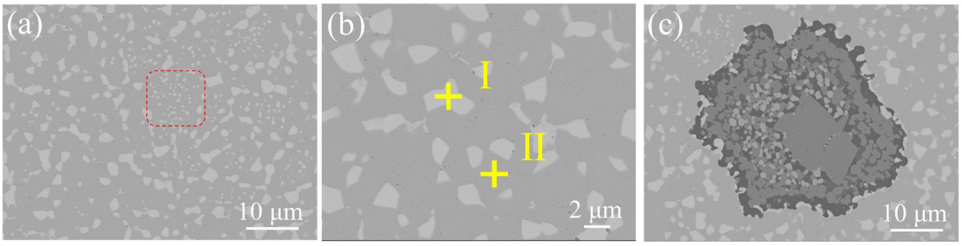

Figure 6: (a) SEM-BSE image of the microstructure in N-HT alloy, (b) the magnification, and (c) the irregular black-gray region.

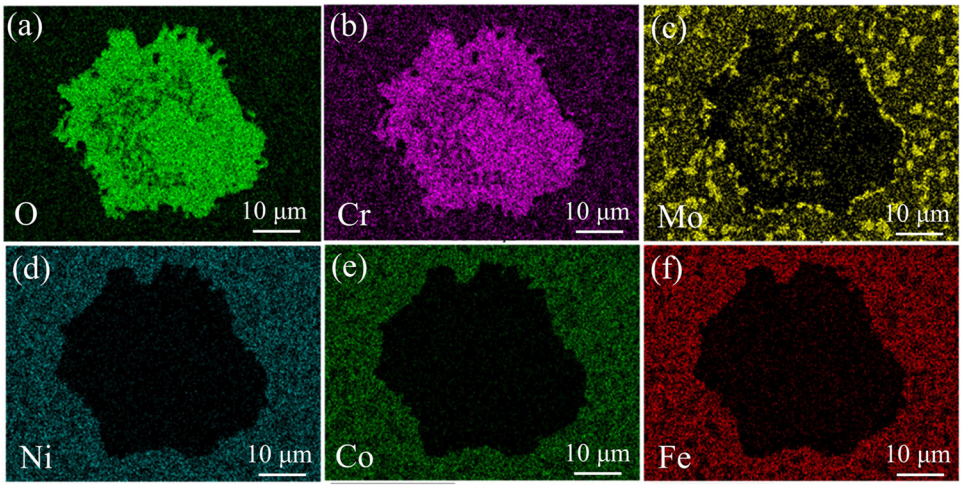

Figure 7: SEM-EDS images of the microstructure in N-HT alloy: (a) distribution of O element, (b) distribution of Cr element, (c) distribution of Mo element, (d) distribution of Ni element, (e) distribution of Co element, and (f) distribution of Fe element.

To investigate the thermal stability of as-sintered $Co_{28.5}Cr_{21.5}Fe_{20}Ni_{26}Mo_4$ MEAs at low temperature, the alloys are annealed at 500, 550, and 600°C. The microstructure of as-annealed $Co_{28.5}Cr_{21.5}Fe_{20}Ni_{26}Mo_4$ MEAs is observed by SEM, and the results are shown in Figure 8a–c. Compared with the as-sintered alloys, the

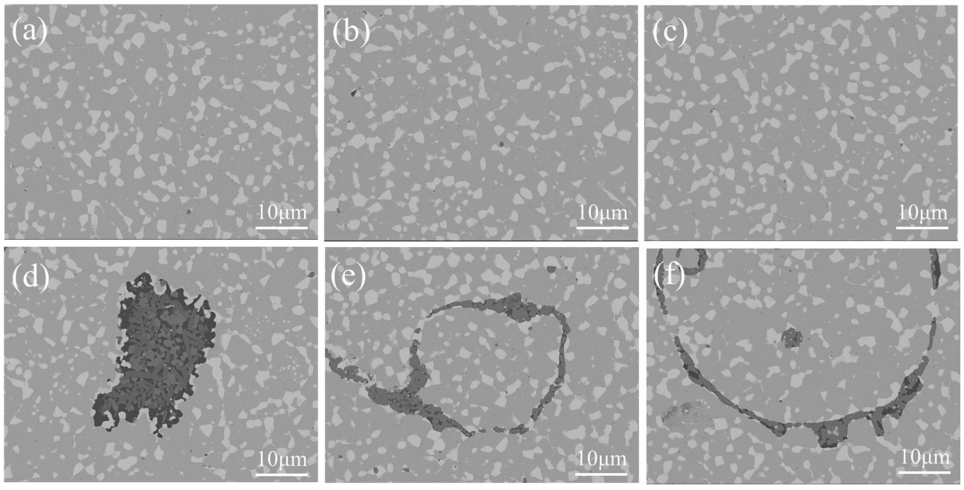

Figure 8: The SEM-BSE images of the microstructure in as-annealed alloys: (a) L-50 alloy, (b) L-55 alloy, (c) L-60 alloy, (d) L-50 alloy, (e) L-55 alloy, and (f) L-60 alloy.

Table 2: Chemical composition of the μ phase and FCC phase in the as-sintered and as-annealed alloys (at%)

Annealing temperature	Phase	Co	Cr	Fe	Ni	Mo
No	μ	20.6 ± 0.6	20.6 ± 0.5	11.0 ± 0.5	15.6 ± 0.8	32.2 ± 0.4
	FCC	28.2 ± 0.7	21.7 ± 0.4	21.3 ± 0.6	25.6 ± 0.6	3.2 ± 0.5
500	μ	20.1 ± 0.5	20.5 ± 0.6	10.3 ± 0.4	15.6 ± 1.0	33.5 ± 0.6
	FCC	28.0 ± 0.7	21.5 ± 0.4	20.4 ± 0.6	25.8 ± 0.9	4.3 ± 0.4
550	μ	21.2 ± 0.8	21.4 ± 0.3	10.0 ± 0.5	15.8 ± 0.8	31.6 ± 0.5
	FCC	27.6 ± 0.8	22.1 ± 0.4	20.6 ± 0.5	26.1 ± 0.8	3.6 ± 0.4
600	μ	20.4 ± 0.6	20.1 ± 0.3	10.3 ± 0.3	15.4 ± 0.7	33.8 ± 0.5
	FCC	28.1 ± 0.7	21.3 ± 0.5	21.0 ± 0.5	26.2 ± 0.9	3.4 ± 0.7
800	μ	21.3 ± 0.7	20.4 ± 0.7	11.9 ± 0.4	17.8 ± 1.0	28.6 ± 0.6
	FCC	28.4 ± 0.6	21.7 ± 0.4	20.5 ± 0.5	26.2 ± 0.9	3.2 ± 0.3
850	μ	21.2 ± 0.5	20.9 ± 0.6	9.5 ± 0.6	17.1 ± 1.1	31.3 ± 0.6
	FCC	26.5 ± 0.8	21.6 ± 0.4	21.1 ± 0.5	27.1 ± 1.0	3.7 ± 0.4
900	μ	20.4 ± 0.6	20.8 ± 0.3	10.8 ± 0.4	15.7 ± 0.8	32.3 ± 0.5
	FCC	28.8 ± 0.7	21.6 ± 0.4	21.2 ± 0.5	25.7 ± 0.9	2.7 ± 0.3
1,100	μ	20.7 ± 0.6	20.1 ± 0.5	10.6 ± 0.4	16.1 ± 0.9	32.5 ± 0.5
	FCC	28.5 ± 0.7	21.5 ± 0.4	20.7 ± 0.5	26.0 ± 0.8	3.3 ± 0.6
1,150	μ	20.5 ± 0.6	20.1 ± 0.5	11.0 ± 0.7	16.0 ± 1.0	32.4 ± 0.5
	FCC	28.3 ± 0.5	21.2 ± 0.7	21.3 ± 0.4	25.8 ± 0.9	3.4 ± 0.4
1,200	μ	20.1 ± 0.6	20.1 ± 0.3	10.7 ± 0.6	16.1 ± 0.8	33.0 ± 0.5
	FCC	28.4 ± 0.7	21.7 ± 0.5	20.6 ± 0.4	25.6 ± 0.9	3.7 ± 0.6

grain distribution of the as-annealed alloys is uniform, and there is no obvious aggregation region of fine μ-phase grains, indicating that the low-temperature annealing can regulate the size and the uniformity of the grains. In addition, as for the alloys annealed at these temperatures, the size and uniformity of the μ phase grains in these alloys is almost consistent with each other, indicating that annealing at low temperature has similar effects on grains. As shown in Figure 8d–f, the irregular black-gray regions are still found in these as-annealed alloys, and these regions display a streamlined shape at 550 and 600°C. Combined with the previous results of the XRD analysis, the irregular region is still mainly comprised Cr_3O_4. However, compared with the irregular black-gray regions in as-sintered alloys, the Mo solid solution virtually disappears, indicating that annealing heat treatment is beneficial for the diffusion of the Mo element into the matrix. The SEM-EDS tests are conducted on as-annealed alloys, and the chemical compositions of the FCC phase and μ phase are presented in Table 2. Meanwhile, the change situation of Fe, Co, Ni, Cr, and Mo elements is shown in Figure 9. Compared with as-sintered alloys, the contents of Fe, Co, Ni, Cr, and Mo elements in the FCC phase and μ phase do not change much, indicating that annealing at low temperature has no obvious influence on the chemical composition of microstructure in$Co_{28.5}Cr_{21.5}Fe_{20}Ni_{26}Mo_4$ MEAs.

To investigate the thermal stability of as-sintered $Co_{28.5}Cr_{21.5}Fe_{20}Ni_{26}Mo_4$ MEAs at moderate temperatures, the alloys are annealed at 800, 850, and 900°C respectively. The SEM-BSE images of the microstructure in as-annealed alloys are shown in Figure 10a–c. Compared with as-sintered alloys, as the temperature increases from 800 to 900°C, the grains of as-annealed alloys gradually become denser and more uniform. The alloys annealed at 800, 850, and 900°C are subjected to the SEM-EDS analysis. The elemental compositions of the FCC phase and μ phase are presented in Table 2, and the change situation of Fe, Co, Ni, Cr, and Mo elements is shown in Figure 9. Compared with as-sintered alloys, the content of each element in the FCC phase does not change much. The Ni element has a slight increase at 850°C (~1.5 at%), and the Co element has a slight decrease at 850°C (~1.7 at%). Similarly, compared with as-sintered alloys, the content of each element in the μ phase still does not alter much. The Mo element has a slight decline at 800°C (~3.6 at%), the Fe element has a slight decline at 850°C (~1.5 at%), and the Ni element has a slight increase at 800°C (~2.2 at%). In addition, there is no significant change in Cr and Co elements.

To evaluate the thermal stability of as-sintered $Co_{28.5}Cr_{21.5}Fe_{20}Ni_{26}Mo_4$ MEAs at high temperature, as-sintered alloys are annealed at 1,100, 1,150, and 1,200°C, respectively. As shown in Figure 10d–f, with the increase of annealing temperature, the grains in as-annealed alloys gradually become sparse, indicating that annealing at a high temperature can contribute to the formation of the FCC phase. In terms of the alloys

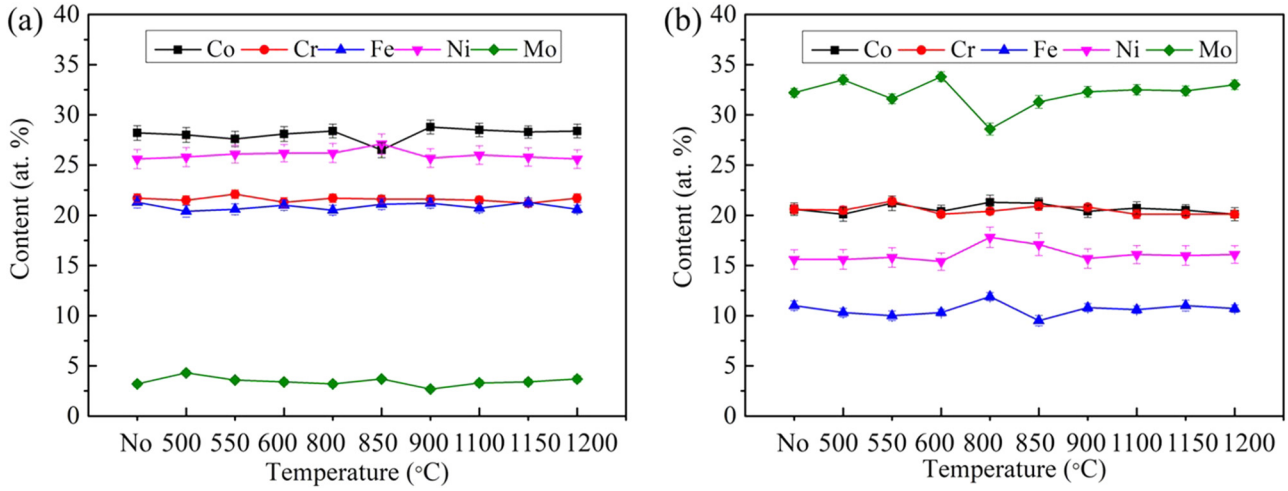

Figure 9: Chemical composition of different phases in the as-sintered and as-annealed $Co_{28.5}Cr_{21.5}Fe_{20}Ni_{26}Mo_4$ MEAs: (a) FCC phase and (b) μ phase.

annealed at high temperature, the size and distribution of the μ phase grains change significantly compared to as-sintered alloys. Furthermore, it can be found that there are no aggregation regions of fine μ phase grains. Then, alloys annealed at 1,100, 1,150, and 1,200°C are subjected to the SEM-EDS analysis. The results are presented in Table 2, and change situation of elements is shown in Figure 9. For the alloys annealed at high temperature, compared with as-sintered alloys, there is no significant change in the content of various elements in the FCC phase and μ phase. Hence, the MEAs have excellent thermal stability at high temperature.

The elemental distribution of $Co_{28.5}Cr_{21.5}Fe_{20}Ni_{26}Mo_4$ MEAs annealed at 1,150°C is studied by the map scanning analysis of EDS, and the results are shown in Figure 11. It is found that the C element mainly distributes in black particles, which is mainly caused by the improper processing during polishing. Mo element is concentrated in the μ phase, while Fe, Co, Ni, and Cr elements are mainly distributed in the FCC phase. In addition, some Co, Ni, and Cr elements are detected in the μ phase, and a small amount of the Fe element can also be detected in the μ phase. Hence, the μ phase is the Mo-rich phase composed of Mo, Cr, Ni, Co, and Fe elements, and the FCC phase is the solid solution phase mainly composed of Fe, Cr, Ni, and Co elements.

As for as-sintered $Co_{28.5}Cr_{21.5}Fe_{20}Ni_{26}Mo_4$ MEAs, both the FCC phase and μ phase are saturated in alloys. After

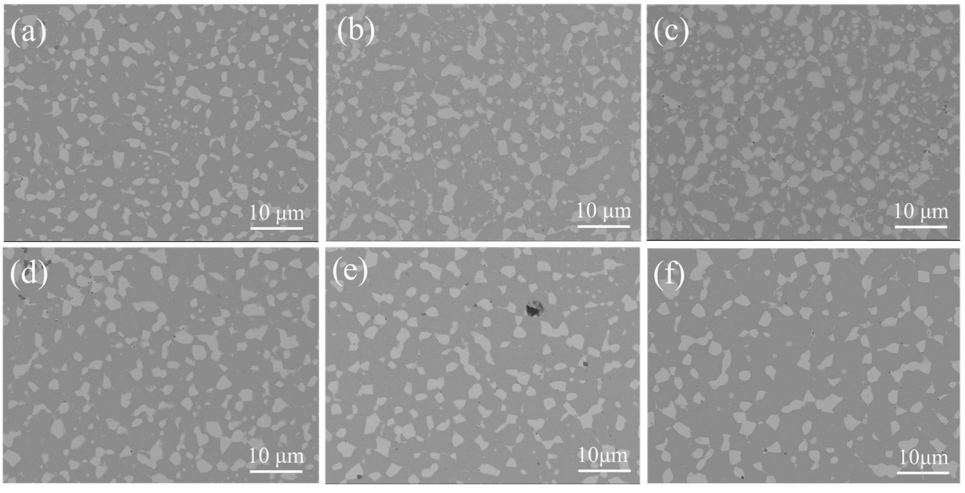

Figure 10: The SEM-BSE images of the microstructure in as-annealed alloys: (a) M-80 alloy, (b) M-85 alloy, (c) M-90 alloy, (d) H-110 alloy, (e) H-115 alloy, and (f) H-120 alloy.

undergoing annealing heat treatment, the change in the size of μ phase grains is mainly related to the solid solubility of elements at different temperatures. Hence, when as-sintered $Co_{28.5}Cr_{21.5}Fe_{20}Ni_{26}Mo_4$ MEAs are annealed, the solute will be redistributed, which results in alteration of the content of the μ phase and FCC phase [43]. In this work, it is necessary to study the ratio change of the μ phase and FCC phase in as-sintered and as-annealed alloys. By using the image processing software Image J [44], the contents of the μ phase and FCC phase in as-sintered and as-annealed alloys are analyzed, and the results are presented in Table 3. It can be found that annealing at low temperature (500, 550 and 600°C) has the similar influence on the content of the μ phase, and the amount of the FCC phase is decreased by 4–5% compared to that of as-sintered alloys. However, compared with as-sintered alloys, when the annealing temperature increases from 800 to 900°C, the content of the FCC phase gradually decreases, and the content of the FCC phase reaches to the minimum value at 900°C (68.38%). This phenomenon indicates that the formation of the μ phase can be promoted at 900°C, and Bae et al. [23] have the similar results in their experiments. In addition, the content of the FCC phase increases with the increase of temperature, and then, its content reaches to the maximum value at 1,200°C (82.42%). Therefore, as presented in Table 3, the fluctuation of the content of the FCC phase and μ phase is relatively large at the annealing temperature of 900 and 1,100°C. The ratio of the FCC phase and μ phase is relatively stable at other temperatures. In particular, the content of the FCC phase does not basically alter compared with that of as-sintered alloys when the annealing temperature is 1,200°C.

3.4 Hardness analysis of $Co_{28.5}Cr_{21.5}Fe_{20}Ni_{26}Mo_4$ MEAs

As a new alloy, the mechanical properties of MEAs are vital for industrial applications. In the current study, hardness is a good indicator for the evaluation of their properties. During the measurement, five test points are randomly selected on the surface of the alloys to determine the hardness value of $Co_{28.5}Cr_{21.5}Fe_{20}Ni_{26}Mo_4$ MEAs. Figure 12 shows the effect of different annealing temperatures on the hardness of $Co_{28.5}Cr_{21.5}Fe_{20}Ni_{26}Mo_4$ MEAs. Compared with the conventional alloys, MEAs can obtain higher hardness at a lower cost [45]. As shown in Figure 12, the hardness value of as-sintered alloys is 342 HV. When the annealing temperature is 500 and 600°C, compared with as-sintered alloys, the value of hardness does not change significantly. However, when the annealing temperature is 550°C, the value of hardness increases to 355 HV, which is attributed to the enhancement of the proportion of the μ phase at this temperature (Table 3). The presence of the μ phase can boost the hardness of the material, and its hardness can reach 15 GPa [17]. The value of hardness gradually increases with the increment of annealing temperature from 800 to 900°C, and the value of hardness reaches the highest at 900°C (370 HV) because of the gradual increase of the μ phase. In the study on Fe–Co–Cr–Ni–Mo_x multielement alloy claddings, Chen et al. [46] found that the Mo element in the μ phase could enhance the hardness of the alloys by precipitation strengthening and solid solution strengthening. As the annealing temperature gradually increases from 1,000 to 1,200°C, the value of hardness gradually decreases and the

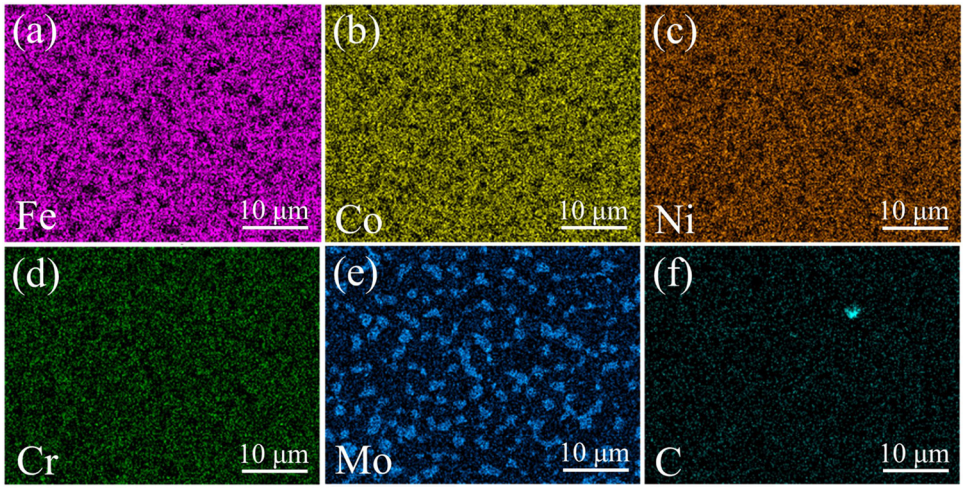

Figure 11: SEM-EDS images of the microstructure in H-115 alloy: (a) distribution of Fe element, (b) distribution of Co element, (c) distribution of Ni element, (d) distribution of Cr element, (e) distribution of Mo element, and (f) distribution of C element.

Table 3: The content of FCC phase and μ phase in as-sintered and as-annealed $Co_{28.5}Cr_{21.5}Fe_{20}Ni_{26}Mo_4$ MEAs (surface%)

Specimen	—	500	550	600	800
FCC	81.56 ± 1.37	77.35 ± 0.96	76.12 ± 1.00	77.99 ± 1.19	79.54 ± 0.80
μ	18.44 ± 1.37	22.65 ± 0.96	23.88 ± 1.00	22.01 ± 1.19	20.46 ± 0.80
Specimen	**850**	**900**	**1,100**	**1,150**	**1,200**
FCC	75.15 ± 1.02	68.38 ± 0.88	76.11 ± 2.07	80.72 ± 1.37	82.42 ± 1.43
μ	24.85 ± 1.02	31.62 ± 0.88	23.89 ± 2.07	19.28 ± 1.37	17.58 ± 1.43

minimum value of 312 HV is obtained at 1,200°C, which is caused by the gradual diminishing of the μ phase (Table 3). However, as for alloys annealed at 1,100°C (as shown in Table 3), although the amount of the μ phase is 23.89%, the value of hardness does not significantly change compared to as-sintered alloys (μ phase: 18.44%). Similarly, compared with as-sintered alloys, although the amounts of the μ phase in the alloys annealed at 1,150 and 1,200°C are 19.28% and 17.58%, respectively, the hardness of these alloys is lower. This abnormal phenomenon is mainly caused by the growth of grains at high temperature. Therefore, although the content of the μ phase can affect the hardness of alloys, the hardness of as-annealed alloys does not change much, indicating that the annealing heat treatment has no significant influence on the hardness of $Co_{28.5}Cr_{21.5}Fe_{20}Ni_{26}Mo_4$ MEAs.

3.5 Analysis of compression properties of $Co_{28.5}Cr_{21.5}Fe_{20}Ni_{26}Mo_4$ MEAs

In this study, since the specimens do not show the trend of fracture during the trial compression tests, the alloys possess excellent compression properties. To avoid damaging the test equipment, compressive strength of 50% strain is selected to conduct comparative analysis [47,48]. Figure 13 shows the compressive strength of as-annealed MEAs and as-sintered MEAs. As shown in Figure 13a–c, compared with as-sintered alloys, as-annealed alloys have a small fluctuation about compressive strength. Figure 13d shows that the average compressive strength of as-sintered alloys is about 2,606 MPa. When the annealing temperature is 600°C, the average compressive strength increases to the highest value of 2,640 MPa. When the annealing temperature is 1,150°C, the average compressive strength of as-annealed alloys decreases to the lowest value of 2,436 MPa. However, when the alloys are annealed at 500, 550, 800, 850, 900, 1,100, and 1,200°C, the compressive strength of as-annealed alloys is almost the same as as-sintered alloys. Hence, there is a small difference in the compressive strength between as-sintered alloys and as-annealed alloys, indicating that $Co_{28.5}Cr_{21.5}Fe_{20}Ni_{26}Mo_4$ MEAs have strong thermal stability in this study. Both as-sintered and as-annealed $Co_{28.5}Cr_{21.5}Fe_{20}Ni_{26}Mo_4$ MEAs have excellent compression properties, and their microstructure is mainly composed of the FCC phase and μ phase. Since the FCC phase has low strength and good plasticity, the $Co_{28.5}Cr_{21.5}Fe_{20}Ni_{26}Mo_4$ MEAs possess excellent plasticity [49]. Moreover, the μ phase existing in the FCC phase matrix does not undergo plastic shear caused by the gliding dislocation during the plastic deformation of the material [50]. Hence, the μ phase can prevent the movement of dislocations to increase the compressive strength of $Co_{28.5}Cr_{21.5}Fe_{20}Ni_{26}Mo_4$ MEAs. In addition, the ductile FCC phase matrix can effectively suppress the crack propagation, and so the MEAs in this study have excellent ductility [23].

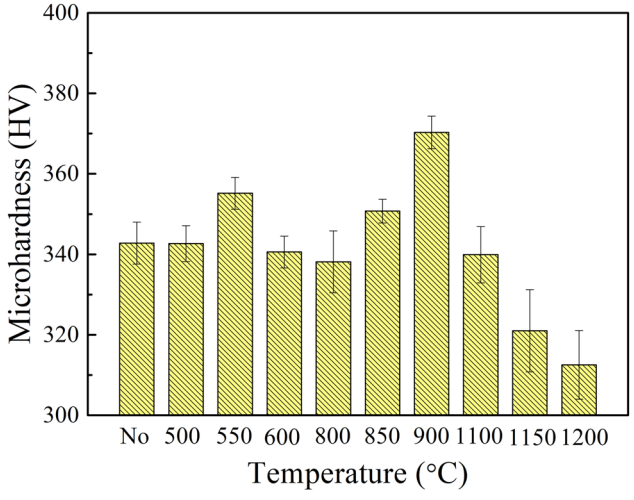

Figure 12: Hardness values of the as-sintered and as-annealed alloys.

4 Discussion

The purpose of this study is to analyze the effect of annealing heat treatment on the microstructure and

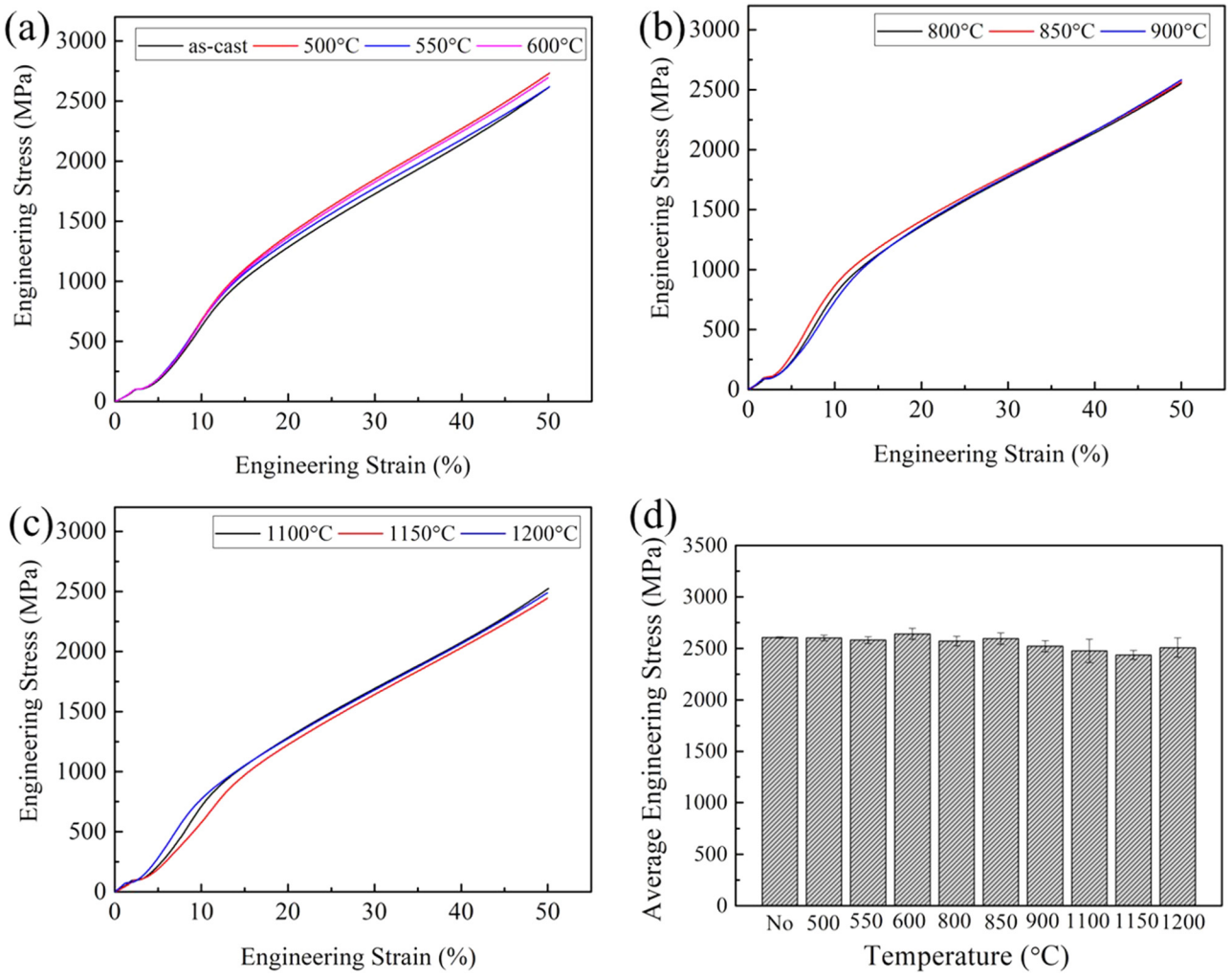

Figure 13: (a) Stress–strain curves of N-HT alloy, L-50 alloy, L-55 alloy, and L-60alloy; (b) stress–strain curves of M-80 alloy, M-85 alloy, and M-90 alloy; (c) stress–strain curves of H-110 alloy, H-115 alloy, and H-120 alloy; and (d) average compressive strength of as-sintered and as-annealed $Co_{28.5}Cr_{21.5}Fe_{20}Ni_{26}Mo_4$ MEAs.

mechanical properties of nonequiatomic $Co_{28.5}Cr_{21.5}Fe_{20}Ni_{26}Mo_4$ MEAs, which are composed of the μ phase and FCC phase, as well as to explore their thermal stability. In the previous studies, it was found that when configurational entropy of the alloy was between 1*R* and 1.5*R* ($R = 8.314\ J\ mol^{-1}\ K^{-1}$), the alloy could be identified as MEA. The mixed entropy of the $Co_{28.5}Cr_{21.5}Fe_{20}Ni_{26}Mo_4$ MEAs can be calculated by the formula (4), and its value is $12.3795\ J\ mol^{-1}\ K^{-1}$ (1.489*R*), and thus, the alloy belongs to MEA. In this work, the formation of phases in the MEAs can be judged by the valence electron concentration of the alloys and the atomic size. From view of the atomic size, the atomic radius of Fe, Co, Ni, and Cr atoms is 1.241, 1.251, 1.246, and 1.249 Å, respectively, and they have the identical valence and electronegativity, which is beneficial for producing simple solid solution between them [51]. Hence, FCC solid solution in the $Co_{28.5}Cr_{21.5}Fe_{20}Ni_{26}Mo_4$ MEAs is mainly composed of Fe, Cr, Ni, and Co elements. However, since the atomic radius of the Mo element (1.363 Å) is significantly larger than that of Fe, Ni, Co, and Cr elements, the Mo element can easily form an intermetallic compound with other elements. Hence, a Mo-rich phase is produced and disperses in the FCC phase matrix. According to the investigation by Guo and Liu [52], the valence electron concentration (VEC) of the alloy plays an important role in the production of the FCC phase and/or BCC phase. If the VEC ≥ 8, it is beneficial for forming the FCC solid solution. If the VEC < 6.87, it is easier to form a BCC solid solution. The VEC values of Fe, Ni, and Co elements are 8, 10, and 9, respectively, indicating that these elements are FCC phase stabilizer. The Ni element is the strongest FCC phase stabilizer. Because the VEC value of Cr and Mo elements is 6, they belong to the BCC phase stabilizer. In this study, the VEC value of $Co_{28.5}Cr_{21.5}Fe_{20}Ni_{26}Mo_4$ MEAs is

8.295, which confirms the presence of the FCC phase. The formula for calculating the VEC is as follows [39,52]:

$$\mathrm{VEC} = \sum_{i=1}^{n} c_i \mathrm{VEC}_i \quad (2)$$

where VEC_i is the VEC of each component and c_i is the concentration of each component in $Co_{28.5}Cr_{21.5}Fe_{20}Ni_{26}Mo_4$ MEAs.

In addition, the formation and the stability of the solid solution can be predicted by the enthalpy of mixing, and the previous studies found that the formation of phases and the segregation of the elements could be determined by the enthalpy of mixing between the elements [53,54]. The enthalpy of mixing between the elements is presented in Table 4. Therefore, the formula (3) is used to calculate the enthalpy of mixing.

$$\Delta H_{\mathrm{mix}} = \sum_{i=1, i=j}^{n} \Omega_{ij} C_i C_j, \ \Omega_{ij} = 4\Delta H_{\mathrm{AB}}^{\mathrm{mix}} \quad (3)$$

$$\Delta S_{\mathrm{mix}} = -R \sum_{i=1}^{n} C_i \ln C_i \quad (4)$$

$$\Delta G_{\mathrm{mix}} = \Delta H_{\mathrm{mix}} - T\Delta S_{\mathrm{mix}} \quad (5)$$

where n is the number of elements in the alloys, C_i and C_j are the atomic percentages of the ith and jth elements, respectively, R_i is the atomic radius of the ith element, $\Delta H_{\mathrm{AB}}^{\mathrm{mix}}$ is the enthalpy of mixing of the binary liquid alloys, and R is the gas constant, H is the mixed enthalpy, S is the mixed entropy, and T is the absolute temperature.

In this study, the enthalpy of mixing of the alloys is $-3.9448\ \mathrm{kJ\ mol^{-1}}$. Yang and Zhang [56] found that when the $\Delta H_{\mathrm{mix}} < 0$, one or more compounds can be stably produced in the alloy. The more negative the enthalpy of mixing is, the greater the binding force between the elements is. Therefore, an intermetallic compound (μ phase) is produced in the $Co_{28.5}Cr_{21.5}Fe_{20}Ni_{26}Mo_4$ MEAs. Zhang et al. [57] found that when $-15\ \mathrm{kJ\ mol^{-1}} < \Delta H_{\mathrm{mix}} < 5\ \mathrm{kJ\ mol^{-1}}$, the solid solution can be formed in the alloy. When enthalpy of mixing becomes more negative, dual phase is easier to be produced. At the same time, Bae et al. [23] studied nonequiatomic $Co_{18}Cr_{12.5}Fe_{55}Ni_7Mo_{7.5}$ MEAs and $Co_{17.5}Cr_{12.5}Fe_{55}Ni_{10}Mo_5$ MEAs. The entropy of mixing of the alloys was 10.6238 and $10.5904\ \mathrm{J\ mol^{-1}\ K^{-1}}$, and the enthalpy of mixing of the alloys was −2.282 and $-2.335\ \mathrm{kJ\ mol^{-1}}$, respectively, as presented in Table 5. Furthermore, the microstructure of these alloys is composed of the FCC phase and μ phase. In contrast, the enthalpy of mixing in this alloy is small. Therefore, in this study, the FCC phase and μ phase are more likely to be produced. It can be seen from the calculation of formula (4) that the entropy of mixing of this MEA is $12.3795\ \mathrm{J\ mol^{-1}\ K^{-1}}$. Compared with $Co_{18}Cr_{12.5}Fe_{55}Ni_7Mo_{7.5}$ MEAs and $Co_{17.5}Cr_{12.5}Fe_{55}Ni_{10}Mo_5$ MEAs, the entropy of mixing of $Co_{28.5}Cr_{21.5}Fe_{20}Ni_{26}Mo_4$ MEAs increases and the high entropy effect is stronger, which can inhibit the formation of brittle intermetallic compounds to promote the production of the FCC phase. The high entropy of mixing can significantly reduce the free energy of the alloy, which can reduce the order degree of the macroscopic solid solution to make the alloy more stable [58]. In addition, it can be known from the formula (5) that since this MEA has the larger entropy of mixing and the smaller enthalpy of mixing, the Gibbs free energy becomes smaller and the alloy is more stable at high temperatures. Therefore, in this work, the FCC phase and μ phase in $Co_{28.5}Cr_{21.5}Fe_{20}Ni_{26}Mo_4$ MEAs are stable.

Table 4: The values of $\Delta H_{\mathrm{AB}}^{\mathrm{mix}}$ ($\mathrm{kJ\ mol^{-1}}$) calculated by Miedema's model for atomic pairs between the elements [55]

	Fe	Co	Ni	Cr	Mo
Fe		−1	−2	−1	−2
Co			0	−4	−5
Ni				−7	−7
Cr					0
Mo					

Among the $Co_{18}Cr_{12.5}Fe_{55}Ni_7Mo_{7.5}$ MEAs processed by heat treatment and the $Co_{17.5}Cr_{12.5}Fe_{55}Ni_{10}Mo_5$ MEAs, the maximum ratio of the μ phase in alloys was up to 8.7% [23]. In the present study, the minimum ratio of the μ phase was 17.58% among the as-sintered and as-annealed $Co_{28.5}Cr_{21.5}Fe_{20}Ni_{26}Mo_4$ MEAs (Table 3). Yang and Zhang [56] found that combining the ratio (Ω) of $T_m\Delta S_{\mathrm{mix}}$ and ΔH_{mix} as well as the atomic size mismatch effect (δ) between atoms could judge the formation ability of solid solution and intermetallic compounds in alloys [59,60]. The relevant equations can be written as equations (6)–(8).When the value of δ is in the range of 0.8%–6.6% and the value of Ω is in the range of 1.1 to 229.8, the solid solution will be easily formed in alloys. In addition, it is also found that when the value of Ω is larger and the value of δ is smaller, the solid solution in alloys possesses better stability. As the diminishing of the value of Ω, the intermetallic phases and amorphous phases are apt to be produced. According to equations (6)–(8), the value of δ and Ω can be calculated, and results are listed in Table 5. Compared with $Co_{18}Cr_{12.5}Fe_{55}Ni_7Mo_{7.5}$ MEAs (Ω = 8.96) and $Co_{17.5}Cr_{12.5}Fe_{55}Ni_{10}Mo_5$ MEAs (Ω = 8.59), the value of Ω of the $Co_{28.5}Cr_{21.5}Fe_{20}Ni_{26}Mo_4$ MEAs (Ω = 5.96) becomes smaller, indicating that the

Table 5: The value of ΔH_{mix}, ΔS_{mix}, Ω, and δ for $Co_{28.5}Cr_{21.5}Fe_{20}Ni_{26}Mo_4$, $Co_{17.5}Cr_{12.5}Fe_{55}Ni_{10}Mo_5$, and $Co_{18}Cr_{12.5}Fe_{55}Ni_7Mo_{7.5}$

	ΔH_{mix} (kJ mol^{-1})	ΔS_{mix} (J mol^{-1} K^{-1})	Ω	δ (%)
$Co_{28.5}Cr_{21.5}Fe_{20}Ni_{26}Mo_4$	−3.9448	12.3795	5.96	1.85
$Co_{17.5}Cr_{12.5}Fe_{55}Ni_{10}Mo_5$	−2.335	10.5904	8.59	2.10
$Co_{18}Cr_{12.5}Fe_{55}Ni_7Mo_{7.5}$	−2.282	10.6238	8.96	2.51

amount of solid solution in this alloy is relatively low, while the amount of intermetallic compounds is relatively high. Hence, the content of the μ phase in the $Co_{28.5}Cr_{21.5}Fe_{20}Ni_{26}Mo_4$ MEAs is higher than that in $Co_{18}Cr_{12.5}Fe_{55}Ni_7Mo_{7.5}$ MEAs and $Co_{17.5}Cr_{12.5}Fe_{55}Ni_{10}Mo_5$ MEAs. As presented in Table 5, compared with $Co_{17.5}Cr_{12.5}Fe_{55}Ni_{10}Mo_5$ and $Co_{18}Cr_{12.5}Fe_{55}Ni_7Mo_{7.5}$ MEAs, the value of δ for the $Co_{28.5}Cr_{21.5}Fe_{20}Ni_{26}Mo_4$ MEAs is lower, indicating that the formation of solid solution in this alloy is more stable [52].

$$\Omega = \frac{T_m \Delta S_{mix}}{|\Delta H_{mix}|} \tag{6}$$

$$T_m = \sum_{i=1}^{n} c_i (T_m)_i \tag{7}$$

$$\delta = \sqrt{\sum_{i=1}^{n} c_i \left(1 - \frac{R_i}{R}\right)^2} \tag{8}$$

$$R = \sum_{i=1}^{n} c_i r_i. \tag{9}$$

where T_m is the melting point temperature of the alloy, $(T_m)_i$ is the melting point of the ith component in the alloy, R_i is the atomic radius of the ith element, and n is the number of elements in the alloy.

In this study, when the annealing temperature is 900°C, the hardness of the $Co_{28.5}Cr_{21.5}Fe_{20}Ni_{26}Mo_4$ MEAs increases to the largest value of 370 HV. When the annealing temperature increases to 1,200°C, the hardness of the alloys decreases to the lowest value of 312 HV. However, compared with the hardness of as-sintered alloys (342 HV), there is no significant difference and the fluctuation value of hardness is just about 30 HV. Therefore, the hardness of $Co_{28.5}Cr_{21.5}Fe_{20}Ni_{26}Mo_4$ MEAs is relatively stable. In addition, when the annealing temperature is 1,150°C, the compressive strength of $Co_{28.5}Cr_{21.5}Fe_{20}Ni_{26}Mo_4$ MEAs decreases to the lowest value of 2,436 MPa. However, when the annealing temperature is 600°C, the compressive strength increases to the highest value of 2,640 MPa. Hence, compared with as-sintered alloys (2,606 MPa), the compressive strength of as-annealed alloys has no significant fluctuation, which demonstrates that the compressive strength of $Co_{28.5}Cr_{21.5}Fe_{20}Ni_{26}Mo_4$ MEAs is relatively stable. Compared with as-sintered alloys, the phase composition of microstructure in as-annealed alloys is still composed of the FCC phase and μ phase. Therefore, the hardness and compressive strength of the as-annealed alloys do not change heavily. Meanwhile, as shown in Figure 9, the alteration of chemical composition of the phase in the as-annealed alloys is just small, indicating that Fe, Co, Ni, Cr, and Mo elements possess low diffusivity at low, medium, and high temperatures [61]. Hence, according to the aforementioned analysis, the $Co_{28.5}Cr_{21.5}Fe_{20}Ni_{26}Mo_4$ MEAs have excellent thermal stability.

5 Conclusions

In this study, the nonequiatomic $Co_{28.5}Cr_{21.5}Fe_{20}Ni_{26}Mo_4$ MEAs produced by hot isostatic pressing sintering were proposed. The effect of the annealing heat treatment on microstructure and mechanical properties of MEAs was investigated. Meanwhile, the thermal stability of $Co_{28.5}Cr_{21.5}Fe_{20}Ni_{26}Mo_4$ MEAs was also evaluated. The relevant conclusions are as follows:

1. The configurational entropy of $Co_{28.5}Cr_{21.5}Fe_{20}Ni_{26}Mo_4$ MEAs was 12.3795 J mol^{-1} K^{-1} (1.489R), the VEC value of MEAs was 8.295, the ΔH_{mix} of MEAs was −3.9448 kJ mol^{-1}, the Ω value of MEAs was 5.96, and the δ value of MEAs was 1.85%.
2. The microstructure of $Co_{28.5}Cr_{21.5}Fe_{20}Ni_{26}Mo_4$ MEAs was mainly composed of the FCC phase and μ phase. The FCC phase was a solid solution phase, which mainly consists of Fe, Co, Ni, and Cr elements, and the μ phase was a (Mo, Cr) rich phase.
3. The $Co_{28.5}Cr_{21.5}Fe_{20}Ni_{26}Mo_4$ MEAs exhibited excellent compression properties (the average value of the compressive strength of as-sintered alloys was 2,606 MPa when the strain was 50%). The presence of the μ phase was beneficial for the improvement of the compression resistance of $Co_{28.5}Cr_{21.5}Fe_{20}Ni_{26}Mo_4$ MEAs. In addition, since the ductile FCC phase could effectively suppress the crack propagation, the ductility of $Co_{28.5}Cr_{21.5}Fe_{20}Ni_{26}Mo_4$ MEAs could be improved.
4. Compared with as-sintered alloys, the phase composition in as-annealed alloys was still composed of the FCC phase and μ phase. In addition, compared with the hardness of as-sintered alloys (342 HV), the fluctuation value of hardness in as-annealed alloys was just ±30 HV. At the same time, when compared

with as-sintered alloys, the compressive strength of as-annealed alloys did not change heavily, and the maximum value of fluctuation was just about 6.5%. Therefore, the thermal stability of $Co_{28.5}Cr_{21.5}Fe_{20}Ni_{26}Mo_4$ MEAs was excellent.

Acknowledgment: This work was supported by Key Laboratory of Infrared Imaging Materials and Detectors, Shanghai Institute of Technical Physics, Chinese Academy of Sciences (No. IIMDKFJJ-19-08) and China Postdoctoral Science Foundation (No. 2015M570794 and 2018T110993).

Conflict of interest: The authors declare that there is no conflict of interest regarding the publication of this article.

References

[1] Li H, Zhang X, Liu QJ, Liu YY, Liu HF, Wang XQ, et al. First-principles calculations of mechanical and thermodynamic properties of tungsten-based alloy. Nanotechnol Rev. 2019;8:258–65.
[2] Zhang XH, Zhang Y, Tian BH, Song KX, Liu P, Jia YL, et al. Review of nano-phase effects in high strength and conductivity copper alloys. Nanotechnol Rev. 2019;8:383–95.
[3] Zhang Y, Zuo TT, Tang Z, Gao MC, Dahmen KA, Liaw PK, et al. Microstructures and properties of high-entropy alloys. Sci Prog Mater Sci. 2014;61:1–93.
[4] Tong CJ, Chen YL, Chen SK, Yeh JW, Shun TT, Tsau CH, et al. Microstructure characterization of Al_xCoCrCuFeNi high-entropy alloy system with multiprincipal elements. Metall Mater Trans A. 2005;36A:881–93.
[5] Senkov ON, Wilks GB, Miracle DB, Chuang CP, Liaw PK. Refractory high-entropy alloys. Intermetallics. 2010;18:1758–65.
[6] Tsai MH, Yeh JW. High-entropy alloys: a critical review. Mater Res Lett. 2014;2:107–23.
[7] Gali A, George EP. Tensile properties of high- and medium-entropy alloys. Intermetallics. 2013;39:74–78.
[8] Otto F, Dlouhy A, Somsen C, Bei H, Eggeler G, George EP. The influences of temperature and microstructure on the tensile properties of a CoCrFeMnNi high-entropy alloy. Acta Mater. 2013;61:5743–55.
[9] Yao MJ, Pradeep KG, Tasan CC, Raabe D. A novel single phase non-equiatomic FeMnNiCoCr high-entropy alloy with exceptional phase stability and tensile ductility. Scr Mater. 2014; 72-73:5–8.
[10] Ai C, He F, Guo M, Zhou J, Wang ZJ, Yuan ZW, et al. Alloy design, micromechanical and macromechanical properties of CoCrFeNiTa$_x$ eutectic high entropy alloys. J Alloy Compd. 2018;735:2653–62.
[11] He F, Wang ZJ, Niu SZ, Wu QF, Li JJ, Wang JC, et al. Strengthening the CoCrFeNiNb$_{0.25}$ high entropy alloy by FCC precipitate. J Alloy Compd. 2016;667:53–57.
[12] John R, Karati A, Garlapati MM, Vaidya M, Bhattacharya R, Fabijanic D, et al. Influence of mechanically activated annealing on phase evolution in $Al_{0.3}$CoCrFeNi high-entropy alloy. J Mater Sci. 2019;54:14588–98.
[13] Molna D, Vida A, Huang S, Chinh NQ. The effect of cooling rate on the microstructure and mechanical properties of NiCoFeCrGa high-entropy alloy. J Mater Sci. 2019;54:5074–82.
[14] Antonov S, Detrois M, Tin S. Design of novel precipitate-strengthened Al-Co-Cr-Fe-Nb-Ni high-entropy superalloys. Metall MaterTrans A. 2018;49 A:305–20.
[15] Chen LJ, Bobzin K, Zhou Z, Zhao LD, Öte M, Königstein T, et al. Effect of heat treatment on the phase composition, microstructure and mechanical properties of $Al_{0.6}$CrFeCoNi and $Al_{0.6}$CrFeCoNiSi$_{0.3}$ high-entropy alloys. Metals. 2018;8:974.
[16] Lee CF, Shun TT. Effect of Fe content on microstructure and mechanical properties of $Al_{0.5}$CoCrFexNiTi$_{0.5}$ high-entropy alloys. Mater Charact. 2016;14:179–84.
[17] Liu WH, Lu ZP, He JY, Luan JH, Wang ZJ, Liu B, et al. Ductile CoCrFeNiMo$_x$ high entropy alloys strengthened by hard intermetallic phases. Acta Mater. 2016;116:332–42.
[18] Wu QF, Wang ZJ, He F, Li JJ, Wang JC. Revealing the selection of σ and μ phases in CoCrFeNiMo$_x$ high entropy alloys by CALPHAD. J Phase Equilib Diffus. 2018;39:446–53.
[19] Wang JW, Liu Y, Liu B, Wang Y, Cao YK, Li TC, et al. Flow behavior and microstructures of powder metallurgical CrFeCoNiMo$_{0.2}$ high entropy alloy during high temperature deformation. Mater Sci Eng A. 2017;689:233–42.
[20] Cai B, Liu B, Kabra S, Wang YQ, Yan K, Lee PD, et al. Deformation mechanisms of Mo alloyed FeCoCrNi high entropy alloy: in situ neutron diffraction. Acta Mater. 2017;127:471–80.
[21] Shun TT, Chang LY, Shiu MH. Age-hardening of the CoCrFeNiMo$_{0.85}$ high-entropy alloy. Mater Charact. 2013;81:92–96.
[22] Shun TT, Chang LY, Shiu MH. Microstructure and mechanical properties of multiprincipal component CoCrFeNiMo$_x$ alloys. Mater Charact. 2012;70:63–67.
[23] Bae JW, Park JM, Moon J, Choi WM, Lee BJ, Kim HS. Effect of μ-precipitates on the microstructure and mechanical properties of non-equiatomic CoCrFeNiMo medium-entropy alloys. J Alloy Compd. 2019;781:75–83.
[24] Lee SH, Nomura N, Chiba A. Effect of Fe addition on microstructures and mechanical properties of Ni- and C-Free Co-Cr-Mo alloys. Mater Trans. 2007;48:2207–11.
[25] Wang F, Inoue A, Kong FL, Han Y, Zhu SL, Shalaan E, et al. Formation, thermal stability and mechanical properties of high entropy (Fe,Co,Ni,Cr,Mo)-B amorphous alloys. J Alloy Compd. 2018;732:637–45.
[26] Zhang XH, Zhang Y, Tian BH, Jia YL, Liu Y, Song KX, et al. Cr effects on the electrical contact properties of the Al_2O_3-Cu/15W composites. Nanotechnol Rev. 2019;8:128–35.
[27] Varalakshmi S, Rao GA, Kamaraj M, Murty BS. Hot consolidation and mechanical properties of nanocrystalline equiatomic AlFeTiCrZnCu high entropy alloy after mechanical alloying. J Mater Sci. 2010;45:5158–63.
[28] Gao MC, Zheng F, Xu JJ, Zhang SY, Bhosale SS, Gu JJ, et al. Surface modification of nano-sized carbon black for reinforcement of rubber. Nanotechnol Rev. 2019;8:405–14.
[29] Mu YK, Jia YD, Xu L, Jia YF, Tan XH, Yi J, et al. Nano oxides reinforced high-entropy alloy coatings synthesized by atmospheric plasma spraying. Mater Res Lett. 2019;7:312–9.

[30] Munitz A, Meshi L, Kaufman MJ. Heat treatments' effects on the microstructure and mechanical properties of an equiatomic Al-Cr-Fe-Mn-Ni high entropy alloy. Mater SciEng A. 2017;689:384–94.
[31] Liu WH, Wu Y, He JY, Nieh TG, Lu ZP. Grain growth and the hall-petch relationship in a high-entropy FeCrNiCoMn alloy. Scr Mater. 2013;68:526–9.
[32] Zhu C, Lu ZP, Nieh TG. Incipient plasticity and dislocation nucleation of FeCoCrNiMn high-entropyalloy. Acta Mater. 2013;61:2993–3001.
[33] Tsai KY, Tsai MH, Yeh JW. Sluggish diffusion in Co-Cr-Fe-Mn-Ni high entropy alloys. Acta Mater. 2013;61:4887–97.
[34] Karlsdottir SN, Geambazu LE, Csaki I, Thorhallsson AI, Stefanoiu R, Magnus F, et al. Phase evolution and microstructure analysis of CoCrFeNiMo high-entropy alloy for electro-spark-deposited coatings for geothermal environment. Coatings. 2019;9:406.
[35] Vaidya M, Karati A, Marshal A, Pradeep KG, Murty BS. Phase evolution and stability of nanocrystalline CoCrFeNi and CoCrFeMnNi high entropy alloys. J Alloy Compd. 2019;770:1004–15.
[36] Sriharitha R, Murty BS, Kottada RS. Alloying, thermal stability and strengthening in spark plasma sintered Al_xCoCrCuFeNi high entropy alloys. J Alloy Compd. 2014;583:419–26.
[37] Jiang L, Jiang H, Lu YP, Wang TM, Cao ZQ, Li TJ. Mechanical properties improvement of $AlCrFeNi_2Ti_{0.5}$ high entropy alloy through annealing design and its relationship with its particle-reinforced microstructures. J Mater Sci Technol. 2015;31:397–402.
[38] Fellinger MR, Hector JLG, Trinkle DR. Impact of solutes on the lattice parameters and elastic stiffness coefficients of hcp Fe from first-principles calculations. Comp Mater Sci. 2019;164:116–26.
[39] Zhuang YX, Xue HD, Chen ZY, Hu ZY, He JC. Effect of annealing treatment on microstructures and mechanical properties of FeCoNiCuAl high entropy alloys. Mater Sci Eng A. 2013;572:30–35.
[40] Praveen S, Anupam A, Tilak R, Kottada RS. Phase evolution and thermal stability of AlCoCrFe high entropy alloy with carbon as unsolicited addition from milling media. Mater Chem Phys. 2018;210:57–61.
[41] Munitz A, Salhov S, Guttmann G, Derimow N, Nahmany M. Heat treatment influence on the microstructure and mechanical propertiesof $AlCrFeNiTi_{0.5}$ high entropy alloys. Mater Sci Eng A. 2019;742:1–14.
[42] Mu YK, Jia YD, Xu L, Jia YF, Tan XH, Yi J, et al. Nano oxides reinforced high-entropy alloy coatings synthesized by atmospheric plasma spraying. Mater Res Lett. 2019;7–8:312–9.
[43] Zhang ZQ, Song KK, Guo S, Xue QS, Xing H, Cao CD, et al. Optimizing mechanical propertiesof $Fe_{26.7}Co_{26.7}Ni_{26.7}Si_{8.9}B_{11}$ high entropy alloy by inducing hypoeutectic to quasi-duplexmicrostructural transition. Sci Rep. 2019;9:360.
[44] Schneider CA, Rasband WS, Eliceiri KW. NIH image to image J: 25 years of image analysis. Nat Methods. 2012;9:671–5.
[45] El-Hadad S, Ibrahim M, Mourad M. Effect of heat treatment and titanium addition on the microstructure and mechanical properties of cast $Fe_{31}Mn_{28}Ni_{15}Al_{24.5}Ti_x$ high-entropy alloys. Adv Mater Sci Eng. 2019;2019:1–10.
[46] Chen JH, Chen PN, Lin CM, Chang CM, Chang YY, Wu W. Characterization of multi-element alloy claddings manufactured by the tungsten inert gas process. Surf Coat Tech. 2009;203:2983–8.
[47] Bayley T, Reddy S, Fard M. Vehicle crash can FEA model simulation and validation with experiment. Data Nonlinear Eng. 2015;4(2):83–90.
[48] Roy S, Petrova RS, Mitra S. Effect of carbon nanotube (CNT) functionalization in epoxy-CNT composites. Nanotechnol Rev. 2018;7(6):475–85.
[49] Xiao MH, Chen JW, Kang JJ, Chen K, Wu D, Gao N. Effect of heat treatment process on mechanical properties and microstructure of $FeAlCoCrNiTi_{0.5}$ alloy. AipAdv. 2018;8:095322.
[50] MingK BiX, Wang J. Precipitation strengthening of ductile $Cr_{15}Fe_{20}Co_{35}Ni_{20}Mo_{10}$ alloys. Scr Mater. 2017;137:88–93.
[51] Huo WY, Zhou H, Fang F, Xie ZH, Jiang JQ. Microstructure and mechanical properties of $CoCrFeNiZr_x$ eutectic high-entropy alloys. Mater Des. 2017;134:226–33.
[52] Guo S, Liu CT. Phase stability in high entropy alloys: formation of solid-solution phase or amorphous phase. Prog Nat Sci-Mater. 2011;21:433–46.
[53] Hsu US, Hung UD, Yeh JW, Chen SK, Huang YS, Yang CC. Alloying behavior of iron, gold and silver in AlCoCrCuNi-based equimolar high-entropy alloys. Mat Sci Eng A. 2007;460–461:403–8.
[54] Zhang KB, Fu ZY, Zhang JY, Wang WM, Wang H, Wang YC, et al. Microstructure and mechanical properties of $CoCrFeNiTiAl_x$ high-entropy alloys. Mat Sci Eng A. 2009;508:214–9.
[55] Wu PH, Liu N, Yang W, Zhu ZX, Lu YP, Wang XJ. Microstructure and solidification behavior of multicomponent $CoCrCu_xFeMoNi$ high-entropy alloys. Mater Sci Eng A. 2015;642:142–9.
[56] Yang X, Zhang Y. Prediction of high-entropy stabilized solid-solution in multi-component alloys. Mater Chem Phys. 2012;132:233–8.
[57] Zhang Y, Zhou YJ, Lin JP, Chen GL, Liaw PK. Solid-solution phase formation rules for multi-component alloys. Adv Eng Mater. 2008;10:6.
[58] Zhang KB, Fu ZY, Zhang JY, Shi J, Wang WM, Wang H, et al. Annealing on the structure and properties evolution of the CoCrFeNiCuAl high-entropy alloy. J Alloy Compd. 2010;502:295–9.
[59] Kittel C. Introduction to Solid State Physics. 7th ed. New York: Wiley; 1996.
[60] Wang ZJ, Huang YH, Yang Y, Wang JC, Liu CT. Atomic-size effect and solid solubility of multicomponent alloys. Scr Mater. 2015;94:28–31.
[61] Guo J, Tang C, Rothwell G, Li L, Wang YC, Yang QX, et al. Welding of high entropy alloys-a review. Entropy. 2019;21:431.